Journal of Inorganic Biochemistry 199 (2019) 110795

Contents lists available at ScienceDirect

Journal of Inorganic Biochemistry

journal homepage: www.elsevier.com/locate/jinorgbio

Improving biosynthesis of Au—Pd core-shell nanoparticles through *Escherichia coli* with the assistance of phytochelatin for catalytic enhanced chemiluminescence and benzyl alcohol oxidation

Dingkun Zhang[a], Donglin Tang[a], Toshiyoshi Yamamoto[a], Yugo Kato[a], Shiho Horiuchi[a], Shinya Ogawa[a], Esturo Yoshimura[a,b], Michio Suzuki[a,*]

[a] Department of Applied Biological Chemistry, Graduate School of Agricultural and Life Sciences, The University of Tokyo, 1-1-1 Yayoi, Bunkyo-ku, Tokyo 113-8657, Japan
[b] The Open University of Japan, 2-11 Wakaba, Mishima-ku, Chiba-city, Chiba 261-8586, Japan

ARTICLE INFO

Keywords:
Au—Pd core-shell nanoparticles
Biosynthesis
Phytochelatin
Escherichia coli
Chemiluminescence
Benzyl alcohol oxidation

ABSTRACT

In this work, Au—Pd core-shell nanoparticles (NPs) biosynthesized through *Arabidopsis thaliana* phytochelatin synthase-modified *Escherichia coli* (Au-Pd/*At*PCS1-*E. coli*) with catalytic enhanced chemiluminescence (CL) and benzyl alcohol oxidation (BAO) was investigated. Such biosynthesis of Au—Pd core-shell NPs was obviously enhanced due to insertion of the gene sequence of *Arabidopsis thaliana* phytochelatin synthase (*At*PCS1) to a plasmid vector (pET-28b) of *Escherichia coli* (*E. coli*). The obtained *Arabidopsis thaliana* phytochelatin synthase-modified *Escherichia coli* (*At*PCS1-*E. coli*) could generate phytochelatins (PCs, $(\gamma\text{-Glu-Cys})_n$-Gly, $n > 1$) for efficient capture and enrichment of Au^{3+}. The component and morphology of Au—Pd core-shell NPs were checked through X-ray diffraction (XRD), scanning electron microscope (SEM), transmission electron microscopy (TEM) and energy dispersive spectrometer (EDS). Catalytic CL (in H_2O_2-luminol system) and BAO (in H_2O_2-benzyl alcohol system) effect with different experimental conditions were examined, respectively. These results revealed that multifunctional PCs could effectively facilitate biosynthetic process of Au—Pd core-shell NPs with better distribution, higher yield and lower cost while stronger CL intensity and higher conversion could be obtained for further quantitative analysis and application.

1. Introduction

The superior chemical activity of bimetallic nanoparticles to their monometallic counterparts have attracted enormous attentions for many years [1] where the improvement of their properties and characteristics have revealed great advantages and potentials in both theoretical and experimental areas [2]. Among these multifunctional bimetallic structures, Au—Pd core-shell nanoparticles (NPs) have obtained many investigations towards their synthesis and application [3] due to their fascinating features in which the synergistic [4] and tunable [5] effect between these two transition metal NPs have exhibited highly efficient catalytic performance [6]. In addition, such core-shell structure [7] also facilitates decreasing the loading amount of the high cost shell metal (Pd) [8]. It is reported that the Au—Pd core-shell NPs have been applied to catalytic oxidation of CO [9], alcohol [10], benzyl alcohol [11] and phenol [12], etc. Recent researches on Au—Pd core-shell NPs mainly concentrate on enhanced synthesis and further development. Comparatively, traditional synthetic techniques of Au—Pd core-shell NPs mainly concentrate on seed growth-based, template-based, one pot-based, co-reduction-based and potential deposition-based strategies [13], which have realized effective fabrication of Au—Pd core-shell NPs with various morphologies and sizes. However, traditional chemical synthesis always occurs with high temperature and pressure, which on the one hand increases the cost of facility and production process; on the other hand releases excessive toxic waste water and gas to the eco-environment. Therefore, synthesis of Au—Pd core-shell NPs with simplicity, efficiency and environmental friendship remains as a great challenge to be solved.

For providing an effective alternative, serving as a newly-emerging and green synthetic method, generation of nanomaterials through bacteria [14] has been widely investigated and developed [15] where studies on their particular reactivities have shown excellent probability for deeper improvement and further application [16]. Comparing with traditional chemical route, this bacteria-based biosynthetic system has definitely created a novel research area of producing nanomaterials through biochemical methods [17]. It is proven that the structure and reactivity of bacteria could be remained after generation process, which

* Corresponding author.
E-mail address: amichiwo@mail.ecc.u-tokyo.ac.jp (M. Suzuki).

https://doi.org/10.1016/j.jinorgbio.2019.110795
Received 19 May 2019; Received in revised form 25 July 2019; Accepted 31 July 2019
Available online 31 July 2019
0162-0134/

contributes to recycle of bacteria and chemical source for later research [18]. Moreover, such biosynthetic strategy also realized fabrication of nanomaterials (single metal, alloy or composite) with all kinds of multifunctional bacteria [19]. There is no doubt that this biosynthetic technology not only provided an environmental-friendly method for fabrication of nanomaterials [20], but also filled the gap between bioactivity and nanotechnology through biosynthetic strategy [21]. Thus it is expected as an ideal technique of producing nanomaterials under mild and green conditions, which also indicated further technical improvement and condition optimization for subsequent practical application and industrial production [22].

Studies based on above biosynthetic method have shown that *Shewanella oneidensis* [23], *Pichia pastoris* [24], *Desulfovibrio desulfuricans* [25], *Cupriavidus necator* [26] and *Escherichia coli* (*E. coli*) [27] could effectively generate Au—Pd core-shell NPs. However, relatively lower production efficiency due to poor utilization of metal ions has limited its wide application. Therefore, enhanced biosynthesis for higher efficiency and yield is urgently necessary for fabrication of Au—Pd core-shell NPs.

Here in, improved biosynthesis of Au—Pd core-shell NPs through *E. coli* with the assistance of phytochelatins (PCs) for catalytic enhanced chemiluminescence (CL) and benzyl alcohol oxidation (BAO) is investigated. As far as we know, this is the first report of catalytic enhanced CL and BAO by biosynthesized Au—Pd core-shell NPs. It is worth noting that acting as a classical peptide produced by higher plants for detoxification, PCs could efficiently capture, fix and sequester heavy metal ions [28], which offered an excellent strategy for selection, enrichment and application of heavy metal ions [29]. However, existing techniques for production of pure PCs suffered from high cost and low yield. In order to solve this problem, this work will innovatively insert the gene sequence of *Arabidopsis thaliana* phytochelatin synthase (*At*PCS1) to a plasmid vector (pET-28b) [30] to modify the property of *E. coli* [31] so that *At*PCS1 will be expressed and released within the cell [32]. The obtained *At*PCS1 could facilitate transformation of glutathione to produce PCs and subsequent enrichment [33] of Au^{3+} [34] so as to promote the generation process of Au—Pd core-shell NPs [35]. It is believed that the Au—Pd core-shell nanoparticles biosynthesized through *Arabidopsis thaliana* phytochelatin synthase-modified *Escherichia coli* (Au-Pd/*At*PCS1-*E. coli*) could provide traditional chemosynthesis and catalytic application a unique alternative, which also exhibits great possibility for further technological improvement and practical application. Relevant abbreviations are listed in Table 1.

2. Experimental

2.1. Chemicals, materials and pretreatment

E. coli (Rosetta (DE3) pLysS) strain is bought from Novagen, Madison, WI. The gene sequence of *At*PCS1 (RAFL04–14-H04) from *Arabidopsis thaliana* is obtained from Riken BioResource Research Center, Saitama, Japan. pET-28b vector is purchased from Novagen, Madison, WI. $HAuCl_4{\cdot}3H_2O$, K_2PdCl_4, $HCOONH_4$, benzyl alcohol, benzaldehyde, 30% H_2O_2, hexadecyl trimethyl ammonium bromide (CTAB) and Isopropyl-β-D-1-thiogalactopyranoside (IPTG) are obtained from Wako Pure Chemical industries, Japan. NaCl, Tris-HCl, glycerol and Tween20 are bought from Kokusan Chemical Co. Ltd., Japan. Tryptone and yeast are purchased from BD Biosciences Advanced Bioprocessing, Miami, USA. The filter is obtained from Toyo Roshi Kaisha, Ltd., Japan. Double deionized water is used throughout the experiment. All chemical reagents used in this experiment are analytical grade and used without further purification. In addition, the transfer of gene sequence of *At*PCS1 [36], preparation of *Arabidopsis thaliana* phytochelatin synthase-modified *Escherichia coli* (*At*PCS1-*E. coli*), analysis of *At*PCS1 expression and detection of glutathione and PCs are described in detail in our previous work [37]. In addition, relevant abbreviations are listed in Table 1.

Table 1
Table of abbreviations.

CL	chemiluminescence
BAO	benzyl alcohol oxidation
NPs	nanoparticles
At	*Arabidopsis thaliana*
*At*PCS1	*Arabidopsis thaliana* phytochelatin synthase
PCs	phytochelatins
pET-28b	a plasmid vector of *Escherichia coli*
E. coli	*Escherichia coli*
*At*PCS1-*E. coli*	*Arabidopsis thaliana* phytochelatin synthase-modified *Escherichia coli*
Au-Pd/*At*PCS1-*E. coli*	Au-Pd core-shell nanoparticles biosynthesized through *Arabidopsis thaliana* phytochelatin synthase-modified *Escherichia coli*
wt*E. coli*	wild type *Escherichia coli*
Au-Pd/wt*E. coli*	Au-Pd core-shell nanoparticles produced by wild type *Escherichia coli*

2.2. Synthesis of au-Pd/AtPCS1-E. coli

10 μL cryopreserved *At*PCS1-*E. coli* is transferred to 5 mL Luria-Bertani (LB) culture media (1% tryptone, 0.5% yeast and 1% NaCl) for amplification at 37 °C for 12 h, then 200 μL such suspension is added to 40 mL LB culture media for incubation at 37 °C for 2 h. The optical density value at 600 nm (OD_{600}) of above suspension is adjusted to 0.6 and next 400 μL, 10 mM IPTG is added. After incubation at 37 °C for 4 h, the suspension of *At*PCS1-*E. coli* is washed by centrifugation (3000 rpm, 4 °C, 3 min) three times with double deionized water to eliminate LB culture media and finally the *At*PCS1-*E. coli* cells are suspended in 40 mL double deionized water. Subsequently, 300 μL, 0.375 mM $HAuCl_4$ is added and further cultured at 37 °C for 48 h. After that, 300 μL, 0.375 mM K_2PdCl_4 and 800 μL, 0.5 M $HCOONH_4$ are added with incubation at 37 °C for 48 h. After that, the suspension is washed three times and finally suspended in sterilized water. For comparison, we also prepared control samples of Au—Pd core-shell NPs produced by wild type *E. coli* (Au-Pd/wt*E. coli*). The control samples were fabricated in the same method as previous production process through *At*PCS1-*E. coli*.

2.3. Characterizations

XRD patterns of the obtained Au—Pd core-shell NPs are gained by Rigaku RINT 2000 diffractometer with monochromator-filtered Cu Ka radiation (λ = 1.5418 Å) at 40 mV and 40 mA. Ultraviolet-visible (UV–vis) absorption are checked on UV–vis spectrophotometer (Jasco, V-550, Japan) from 400 to 700 nm. SEM (S-4800, Hitachi, Japan with a cold field-emission gun at 15 kV) is used to observe the morphologies of the samples. The internal structure and component of Au—Pd core-shell NPs are characterized by TEM (JEM-2010, JEOL, Japan) with operation at 200 kV and EDS (EX-24025JGT, JEOL, Japan), respectively. Size distribution and average diameter of samples are calculated within 58 Au—Pd core-shell NPs. The concentration of Au^{3+} and Pd^{2+} are determined on inductively coupled plasma atomic emission spectrometer (ICP-AES, SPS-3500, SII Nano Technology, Japan).

2.4. CL test

The obtained Au-Pd/*At*PCS1-*E. coli* or Au-Pd/wt*E. coli* is re-suspended in 40 mL extraction buffers (25 mM Tris-HCl (pH = 8), 400 mM NaCl, 10% glycerol, 0.1% Tween20) in ice bath for ultrasonication treatment to break the structure of cell and release the Au—Pd core-shell NPs inside. The precipitation of such mixture is eliminated by centrifugation. Finally, the supernatant is treated with 0.45 μm filter. The CL is detected by using a luminescence analyzer (ImageQuant Las 4000, General Electric Company, USA) and test time is 2 min. In a typical experiment, 50 μL, 10^{-4} M luminol, 50 μL, 0.1 M

H_2O_2 and 50 μL suspension of Au—Pd core-shell NPs are mixed in a 96-well plate with mild shaking. The image and relevant CL intensity of each well is recorded. Each experiment is repeated three times.

2.5. BAO test

A 5 mL glass bottle containing benzyl alcohol (0.2 mL, 0.25 M), 30% H_2O_2 (2.451 mL), CTAB (36.44 mg) and suspension of Au—Pd core-shell NPs (1 mL) is sealed and kept in a constant temperature (40 °C) water bath with vigorous stirring for 12 h. Then 365 μL above mixture is diluted to 10 mL with acetonitrile for gas chromatography and mass spectrometry (GCMS, Shimadzu-QP2010 SE, Japan) test. The GCMS is equipped with DB-5 capillary column (Agilent, USA). The temperature of column oven, injector port, ion source and interface is 80 °C, 250 °C, 200 °C and 250 °C, respectively. The program of the oven is set as: firstly held at 80 °C for 2 min, then increased to 300 °C at the rate of 30 °C/min and kept for 5 min. Selective ion monitoring is applied to detect benzyl alcohol (*m/z*: 79), benzaldehyde (m/z: 77) and benzoic acid (m/z: 105).

Conversion of benzyl alcohol ($C_{alcohol}$) and selectivity towards benzaldehyde ($S_{aldehyde}$) were calculated as follows:

$$C_{alcohol} = [(C_0 - C_{alcohol})/C_0] \times 100\%$$

$$S_{aldehyde} = [C_{aldehyde}/(C_0 - C_{alcohol})] \times 100\%$$

In these equations, C_0 represents the initial concentration of benzyl alcohol, $C_{alcohol}$ and $C_{aldehyde}$ mean the concentration of the benzyl alcohol and benzaldehyde, respectively. Each experiment is repeated three times.

3. Results and discussions

3.1. Biosynthetic process of Au-Pd/AtPCS1-E. coli

As is shown in Fig. 1, the biosynthetic process of Au-Pd/*At*PCS1-*E. coli* could be divided into eight parts: preculture, amplification, adjustment of OD value, rinse, addition of Au^{3+}, incubation, addition of Pd^{2+} and incubation. During such biosynthetic process, the *At*PCS1-*E. coli* cells are cultured to a certain concentration with optimal activity. Adjustment of OD value have ensured precursors with similar state. IPTG is added to induce expression of *At*PCS1 and generation of PCs. Through such biosynthetic strategy, the Au—Pd core-shell NPs are obtained for later characterization and application. Definitely, *At*PCS1-*E. coli* could remain active after previous amplification and express *At*PCS1 after addition of IPTG during the generation process. The *At*PCS1 will be activated by addition of Au^{3+} and further catalyze production of PCs to collect and enrich Au^{3+} [38]. Meanwhile, *E. coli* itself is responsible for transforming Au^{3+} to Au NPs. Subsequently, precipitation of Pd^{2+} by $HCOONH_4$ occurs on Au NPs (core) and the obtained Pd NPs (shell) cover the surface of Au NPs so that such Au—Pd core-shell structure could be fabricated within *At*PCS1-*E. coli* [39]. Based on above synthetic process, comparing with traditional chemosynthesis, the biosynthesis technique exceeds in economical reactant (*E. coli* cells, LB culture media and chemicals), quick generation process (incubating *E. coli* cells and adding Au^{3+} and Pd^{2+}), simple instruments (sample tube), which has established a time-saving and environmental-friendly biosynthetic strategy [40]. Although it seems that such biosynthetic process is not very simple (eight parts) comparing with traditional chemosynthesis, it is worthwhile to point out that green process together with fewer wastes have definitely shown superior advantages of this novel biosynthetic strategy where great potential is proven to be accessible comparing with existed chemosynthesis.

3.2. XRD patterns of Au-Pd/AtPCS1-E. coli

XRD patterns of the obtained Au-Pd/*At*PCS1-*E. coli* is shown in Fig. 2a. The main diffraction peaks at 38.26°, 44.60°, 64.68° and 77.55° can be indexed to the (111), (200), (220) and (311) diffractions of Au (JCPDS No. 65–2870). Another four peaks centered at 40.12°, 46.66°, 68.13° and 82.11° correspond to the (111), (200), (220) and (311) diffractions of Pd (JCPDS No. 46–1043) [41], which also indicates effective reduction of Au^{3+} and Pd^{2+} to Au and Pd during the biosynthetic process. The relevant broad peaks indicate the small particle size of Au and Pd NPs. Similarly, XRD patterns of Au-Pd/wt*E. coli* (Fig. 2b) also displayed characteristic and broad peaks of Au and Pd NPs.

3.3. Morphology and component characterization of biosynthesized Au-Pd/AtPCS1-E. coli

The morphologies of Au-Pd/*At*PCS1-*E. coli* are observed by SEM

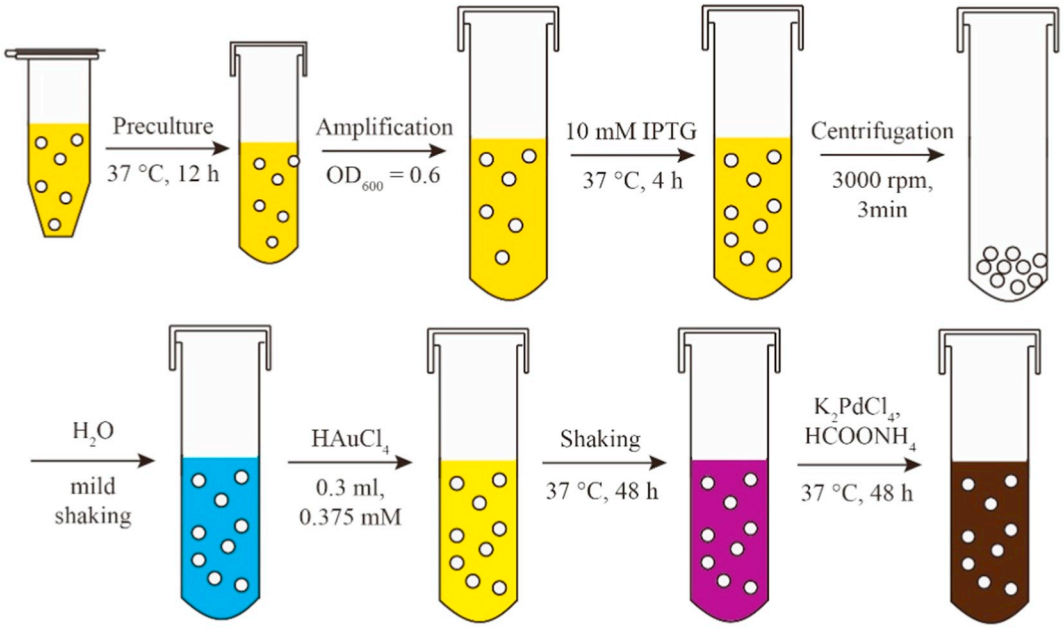

Fig. 1. Biosynthetic process of Au-Pd/*At*PCS1-*E. coli*.

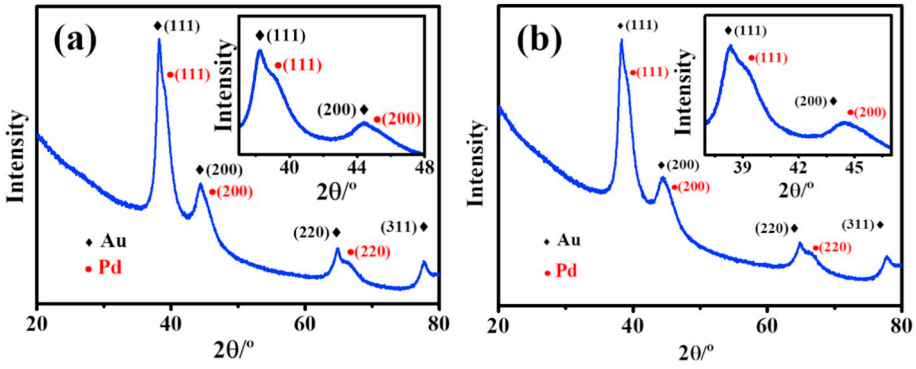

Fig. 2. XRD patterns of (a) Au-Pd/*At*PCS1-*E. coli* and (b) Au-Pd/wt*E. coli*.

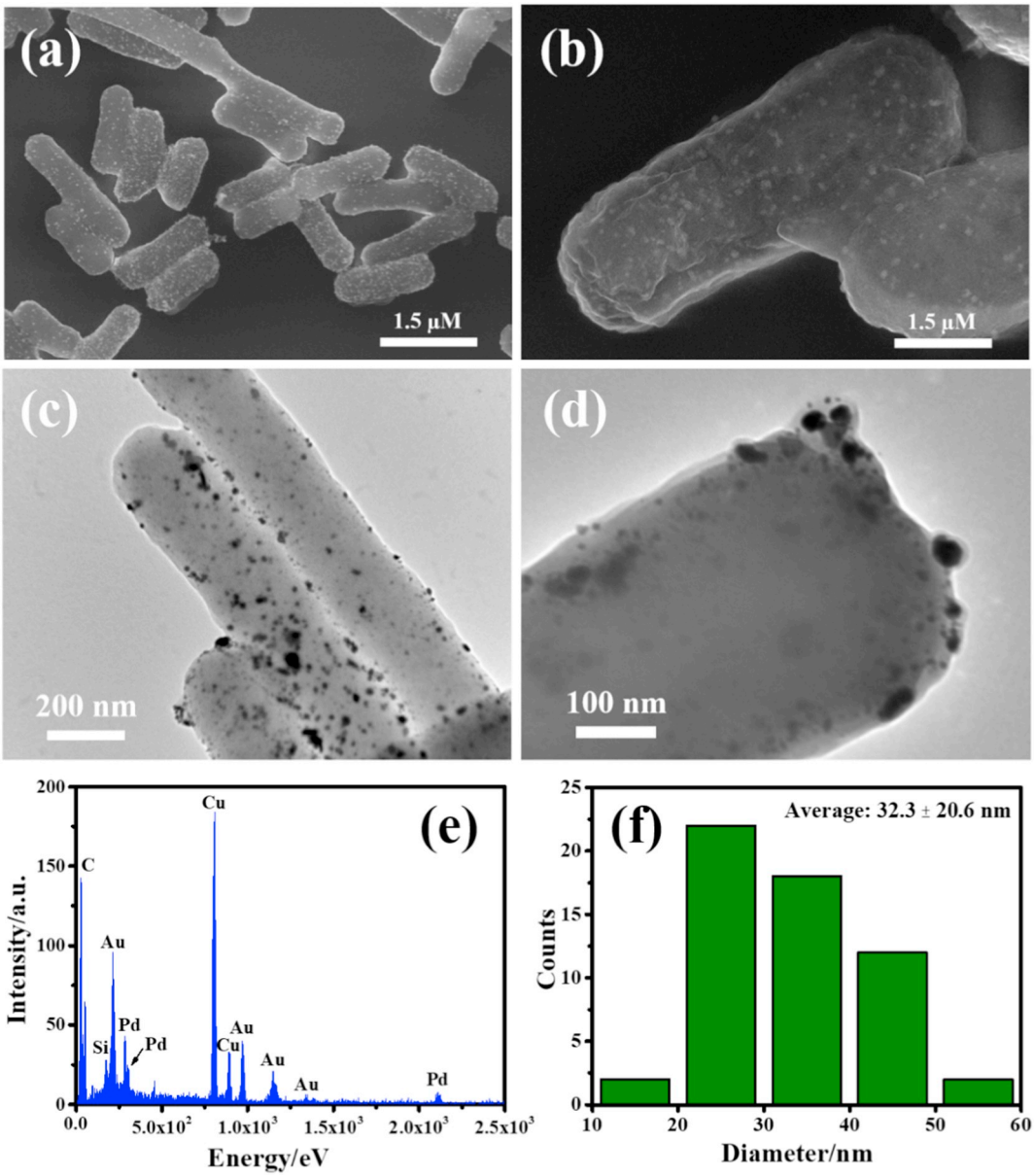

Fig. 3. Morphology and component characterization of Au-Pd/*At*PCS1-*E. coli*. (a) SEM observation; (b) Magnified SEM micrographs; (c) TEM observation; (d) Magnified TEM micrographs; (e) EDS analysis; (f) size distribution and average diameter analysis.

(Fig. 3a and b) that plenty of Au—Pd spherical NPs exist together with *At*PCS1-*E. coli* with fairly well dispersion while there is no Au—Pd core-shell NPs outside of the cell body. TEM images (Fig. 3c and d) not only display these NPs distribute without agglomeration, but also further prove that these NPs locate at the inner surface of the cell. These morphologies are also observed in Au-Pd/wt*E. coli* sample (Fig. S1a–d).

Interestingly, Au and Pd elements could not be detected (Fig. S2b) in the intracellular spaces without NPs (Fig. S2a, white circle), which means that the internal metal ions have been reduced to NPs. It could be deduced that in this biosynthetic system, *E. coli* cells for one thing fabricate Au—Pd core-shell NPs by themselves, for another thing offer sufficient intracellular space so as to prevent unnecessary accumulation of Au—Pd core-shell NPs and better dispersion of them could be acquired [42]. Moreover, EDS analysis (Figs. 3e and S1e) of above system also demonstrates the coexistence of Au and Pd elements. It is notable that the average diameters of Au-Pd/*At*PCS1-*E. coli* is 32.3 nm (Fig. 3f) while Au-Pd/wt*E. coli* is 16.7 nm (Fig. S1f). This longer diameter is ascribed to existence of PCs within *At*PCS1-*E. coli* cells, these PCs have offered a great many active sites for collection and enrichment of Au^{3+} so that more Au—Pd core-shell NPs could be produced. Similarly, higher concentrations of Au^{3+} and Pd^{2+} are also detected in Au-Pd/*At*PCS1-*E. coli* (1.36×10^{-4} M and 2.9×10^{-4} M) than Au-Pd/wt*E. coli* (7×10^{-5} M and 2.56×10^{-4} M) sample through ICP-AES test.

3.4. UV–vis absorption spectra of biosynthesized Au-Pd/AtPCS1-E. coli

The UV–vis absorption spectra of biosynthesized Au-Pd/*At*PCS1-*E. coli* with different concentration of Au^{3+} added are shown in Fig. 4a. It is found that the absorbance intensities raise as the concentration of Au^{3+} increase from 0.125 to 0.5 mM both in the ultraviolet (250 to 400 nm) and visible-light region (> 400 nm), which means that higher concentration of Au^{3+} contributes to increased UV–vis absorbance due to higher yield of Au—Pd core-shell NPs within *At*PCS1-*E. coli* (Fig. S4) [43]. In addition, UV–vis absorption spectra of Pd—Au core-shell NPs with the concentration of Au^{3+} ranging from 0.125 to 0.5 mM (Fig. 4b) indicate that 0.375 mM facilitates highest absorbance. However, the characteristic peak at 550 nm, representative peak of Au NPs, could only be found in Pd—Au core-shell NPs sample because Au NPs exist at the surface of the structure. It is deduced that in Au—Pd core-shell NPs sample, the Au NPs are covered by Pd NPs so that the peak located at 550 nm could not be detected. The above comparisons have further demonstrated the core-shell structure of biosynthesized Au—Pd NPs.

3.5. CL spectra of H_2O_2-luminol system with biosynthesized Au-Pd/AtPCS1-E. coli under different experiment conditions

3.5.1. Condition optimization of H_2O_2-luminol system

The CL spectra of H_2O_2-luminol system as the blank with different experiment conditions are detected and optimized (Fig. S3). It is found that higher concentration of luminol (10^{-4} M) facilitates higher CL intensity (Fig. S3a) and darker CL image (Fig. S3a, inset) where more luminol could be oxidized and excited. In addition, stronger emission is acquired with addition of Au-Pd/*At*PCS1-*E. coli* or Au-Pd/wt*E. coli* than blank sample where disintegration of H_2O_2, evolution of highly reactive ·OH, oxidation of luminol and generation of emissive intermediate could be greatly enhanced through catalysis of Au—Pd core-shell NPs. However, Au-Pd/*At*PCS1-*E. coli* has realized higher CL intensity than Au-Pd/wt*E. coli* owing to higher production of Au—Pd core-shell NPs. The PCs synthesized by *At*PCS1-*E. coli* could efficiently capture and enrich more Au^{3+} within the cell body so that higher yield of Au—Pd core-shell NPs is feasible. Meanwhile, better emissive effect could be obtained with suitable concentration of H_2O_2 (0.5 M) where insufficient H_2O_2 results in fewer excited intermediate while excessive H_2O_2 leads to decomposition of illuminant (Fig. S3b). Similarly, Au-Pd/*At*PCS1-*E. coli* not only does help to stronger emission than blank, but also contributes to higher CL intensity and deeper CL image (Fig. S3b, inset) than Au-Pd/wt*E. coli* with PCs for efficient collection of Au^{3+}.

3.5.2. Different concentrations or interaction time of IPTG

Serving as an indispensable chemical for inducing expression of PCS and production of PCs, IPTG with different concentrations or interaction time on CL effect are detected. As is exhibited in Fig. 5a, when the concentrations of IPTG increases from 2.5 to 10 mM, higher CL intensity of H_2O_2-luminol-Au-Pd/*At*PCS1-*E. coli* system could be attained, which means that 10 mM IPTG is sufficient for expression of PCS by *At*PCS1-*E. coli*. Furthermore, the luminous intensity of all these samples have exceeded the sample without addition of IPTG. It is certain that more IPTG contributes to more PCS expression, production of PCs and fabrication of Au—Pd core-shell NPs. Comparatively, these samples with Au-Pd/*At*PCS1-*E. coli* have shown superior CL performance and darker CL image (Fig. 5a, inset) than with Au-Pd/wt*E. coli* under same experimental conditions. On account of multifunctional PCs, more Au^{3+} could be captured and utilized so that more Au NPs could be generated with deeper purple suspension (Fig. S4a) and stronger UV–vis absorbance at 550 nm (Fig. S5a and b) [44]. The stable CL intensities with Au-Pd/wt*E. coli* in different concentrations of IPTG also indicate the gene sequence of *At*PCS1 do not exist in wild type *Escherichia coli* (wt*E. coli*). In addition, the CL effect of H_2O_2-luminol-Au-Pd/*At*PCS1-*E. coli* system with different interaction time with IPTG revealed increased intensity from 2 to 6 h treatment and remain stable from 6 to 12 h reaction (Fig. 5b), which illustrates that 6 h is suitable for evolution of more PCS, PCs, Au—Pd core-shell NPs and intense purple suspension (Fig. S4b) and more obvious UV–vis absorbance at 550 nm (Fig. S5c and d). It is worth noting that lower CL intensity and lighter CL image (Fig. 5b, inset) with Au-Pd/wt*E. coli* than Au-Pd/*At*PCS1-*E. coli* are also observed and slight increase of CL effect from 2 to 12 h is attributed to slow proliferation of wt*E. coli* together with mild biosynthesis of Au—Pd core-shell NPs.

3.5.3. Different concentration of Au^{3+} and E. coli cells

The CL performance of H_2O_2-luminol-Au-Pd/*At*PCS1-*E. coli* system with different concentration of added Au^{3+} is also checked (Fig. 5c) in

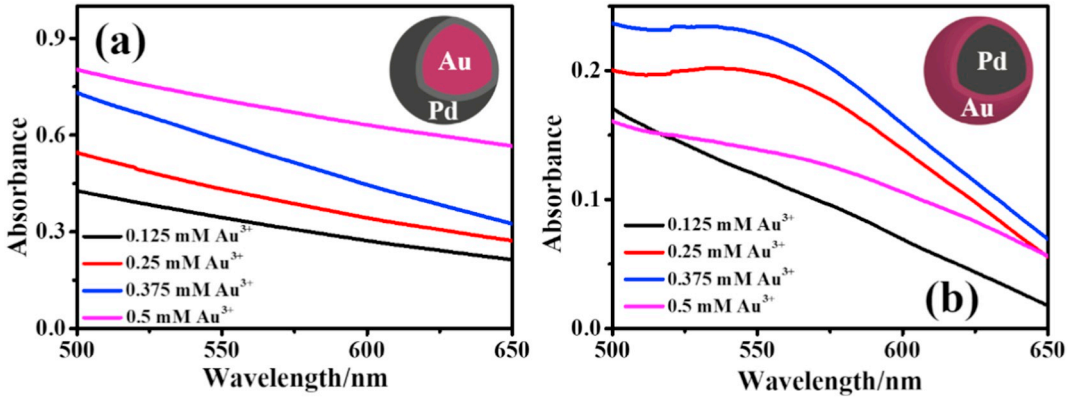

Fig. 4. UV–vis absorption spectra of biosynthesized Au-Pd/*At*PCS1-*E. coli* (a) and Pd-Au/*At*PCS1-*E. coli* (b) with different concentration of Au^{3+}. Inset are core-shell structures of Au—Pd and Pd—Au NPs, respectively.

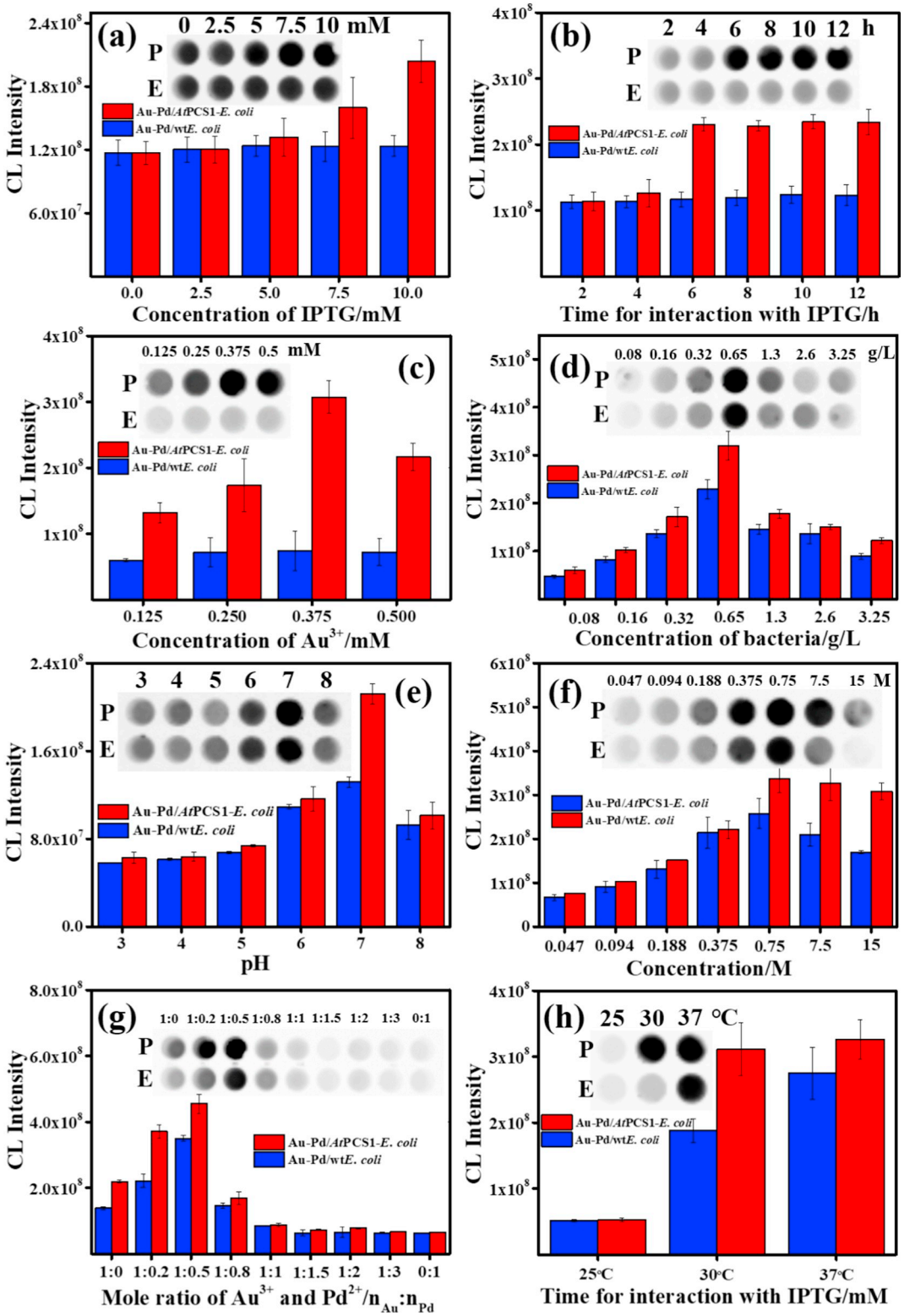

Fig. 5. CL spectra of H_2O_2-luminol system with Au-Pd/*At*PCS1-*E. coli* or Au-Pd/wt*E. coli* under different experiment conditions. Different concentration of (a) concentration and (b) interaction time of IPTG; different concentration of (c) Au^{3+} and (d) *E. coli* cells; (e) different pH; different (f) concentration and (g) mole ratio of Au—Pd core-shell NPs; (h) different temperature. Concentration of luminol: 10^{-4} M, concentration of H_2O_2: 0.5 M. P: with Au-Pd/*At*PCS1-*E. coli*, E: with Au-Pd/wt*E. coli*.

which better CL performance is obtained from 0.125 to 0.375 mM Au^{3+} with higher yield of Au NPs (Fig. S6) while excessive Au^{3+} leads to decreased CL because of fewer Au NPs together with lower cell viability where exposure to excessive amount of Au^{3+} (0.5 mM) results in irreversible cytotoxicity [45]. Similar to previous samples, the CL system with Au-Pd/*At*PCS1-*E. coli* have exhibited preferable glowing effect and darker CL image (Fig. 5c, inset) than with Au-Pd/wt*E. coli* in the same conditions due to poor interaction between Au^{3+} and *E. coli*

cell without the assistance of PCs. Expression of PCS is conducive to efficient absorption and enrichment of Au^{3+} in *At*PCS1-*E. coli* thus higher production of Au—Pd core-shell NPs accompanied with deeper purple suspension (Fig. S4c) and stronger UV–vis absorbance at 550 nm (Fig. S5e and f) are available. Meanwhile, *E. coli* cells not only act as reagent and reactor, but also achieve green biosynthetic process. In Fig. 5d, higher concentration of *At*PCS1-*E. coli* (from 0.08 to 0.65 g/L) brings about enhanced CL effect of H_2O_2-luminol-Au-Pd/*At*PCS1-*E. coli* system, which means that more *At*PCS1-*E. coli* contributes to generation of more PCs and Au—Pd core-shell NPs. However, redundant cells (from 0.65 to 3.25 g/L) give rise to reduced CL intensity, which is attributed to decrease of cellular activity with limited culture media [46]. Similarly, stronger CL emission and deeper CL image (Fig. 5d, inset) with Au-Pd/*At*PCS1-*E. coli* are observed than with Au-Pd/wt*E. coli*. Owing to existence of PCs, darker purple suspension (Fig. S4d) and more evident UV–vis absorbance at 550 nm (Fig. S5g and h) could be gained.

3.5.4. Different pH

It is widely accepted that cellular activity has close relationship with pH value where excessively high or low pH will lead to decreased viability of *E. coli* cells [47]. As is displayed in Fig. 5e, CL performance varies among Au—Pd core-shell NPs fabricated with different pH in H_2O_2-luminol-Au-Pd/*At*PCS1-*E. coli* system where pH level of 7 does help to stronger lighting effect. Moreover, too high or low pH would inevitably inhibit biosynthesis of Au-Pd/*At*PCS1-*E. coli* so that weaker CL could be detected. Notably, because of the presence of PCs, H_2O_2-luminol-Au-Pd/*At*PCS1-*E. coli* system has exhibited more obvious emission and darker CL image (Fig. 5e, inset) than with Au-Pd/wt*E. coli* in the pH value ranging from 3 to 8 while deeper purple suspension (Fig. S4e) and stronger UV–vis absorbance at 550 nm (Fig. S5i and j) could also be observed.

3.5.5. Different concentration and mole ratio of Au-Pd/AtPCS1-E. coli

The CL spectra of H_2O_2-luminol-Au-Pd/*At*PCS1-*E. coli* system with different concentration of Au—Pd core-shell NPs suspension are checked. Satisfactory CL performance could be gained with 0.75 M Au—Pd core-shell NPs where less catalysts give rise to poor interaction and enhancement while more catalysts prevent effective contact and reaction between H_2O_2 and luminol (Fig. 5f). Likewise, Au-Pd/*At*PCS1-*E. coli* facilitates better CL effect and darker CL image (Fig. 5f, inset) than Au-Pd/wt*E. coli* and blank due to existence of intracellular PCs. In addition, investigation of CL effect of H_2O_2-luminol-Au-Pd/*At*PCS1-*E. coli* system with various mole ratios reveal that higher CL intensity could be obtained when mole ratio of Au:Pd increases from 1:0 to 1:0.5 while it decreases from 1:0.5 to 1:3 (Fig. 5g). Definitely, appropriate mole ratio of Au:Pd (1:0.5) facilitates efficient electron transfer so that reaction between H_2O_2 and luminol and evolution of excited intermediate would be greatly improved [48]. Meanwhile, participation of PCs could result in larger amount of biosynthesized Au—Pd core-shell NPs thus the emissive intensity and CL image (Fig. 5g, inset) of samples with Au-Pd/*At*PCS1-*E. coli* have surpassed those with Au-Pd/wt*E. coli*.

3.5.6. Different temperature for fabrication of Au-Pd/AtPCS1-E. coli

A variety of temperature for generation of Au-Pd/*At*PCS1-*E. coli* is studied and shown in Fig. 5h. As the temperature increases from 25 to 37 °C, improved CL performance of H_2O_2-luminol-Au-Pd/*At*PCS1-*E. coli* system is acquired at 37 °C. It is believed that 37 °C contributes to higher cell viability and later biosynthesis [49]. Interestingly, this temperature is identical to the one with previous preculture and amplification step so that the *E. coli* cells with active state could be obtained. Relatively speaking, the emission and CL image (Fig. 5h, inset) of H_2O_2-luminol-Au-Pd/*At*PCS1-*E. coli* have exceeded the system with Au-Pd/wt*E. coli* where evolution of PCs has enabled *At*PCS1-*E. coli* to collect and utilize more Au^{3+} under specific temperature with deeper purple suspension (Fig. S4f) and stronger UV–vis absorbance at 550 nm (Fig. S5k and l) could be detected.

3.6. BAO test of H_2O_2-benzyl alcohol system with biosynthesized Au-Pd/AtPCS1-E. coli under different experiment conditions

Serving as a significant industrial raw material and intermediate with research and productive significance, benzaldehyde has been widely used in fabrication of perfume, herbicides, drug and dye due to its excellent chemical activity [50]. Generally, synthesis of benzaldehyde always occurs through oxidation of benzyl alcohol under controlled conditions where productions with preferable conversion of benzyl alcohol together with selectivity towards benzaldehyde have remained a big challenge for both research and industry [51]. Hence, a catalyst with high reactivity and easy preparation is urgently needed for catalyzing oxidation of benzyl alcohol and generation of benzaldehyde [52].

The GCMS total ions chromatograph (Fig. 6a) of H_2O_2-benzyl alcohol-Au-Pd/*At*PCS1-*E. coli* system reveals that characteristic peaks of benzaldehyde (3.1 min) and benzyl alcohol (3.65 min) could be observed, which indicates that added Au-Pd/*At*PCS1-*E. coli* could facilitate production of benzaldehyde [11]. In addition, through calculation with standard curve method (Fig. S7), the conversion of H_2O_2-benzyl alcohol-catalyst system exhibits that higher concentration of Au^{3+} (0.375 mM) contributes to higher conversion (71.7%) of benzyl alcohol (Fig. 6b) where more Au NPs could be prepared for subsequent catalysis [53]. Comparatively, higher conversion of H_2O_2-benzyl alcohol system with Au-Pd/*At*PCS1-*E. coli* has been detected than with Au-Pd/wt*E. coli* with the concentration of Au^{3+} ranging from 0.125 to 0.5 mM, which is attributed to evolution of PCs so that more biosynthesized Au—Pd core-shell NPs could effectively promote catalytic oxidation of benzyl alcohol [54]. Meanwhile, similar selectivity of these two samples displays that these bimetallic structures could be considered as effective promoters for generation of benzaldehyde [55].

In order to enable a direct proof of remarkable activity of this biosynthesized nanocatalysts, conversion and selectivity of as-prepared Au-Pd/*At*PCS1-*E. coli* with optimum experimental condition (6 h interaction with 10 mM IPTG, addition of 0.375 mM Au^{3+} and 0.65 g/L *At*PCS1-*E. coli*, pH = 7, 0.75 M Au—Pd core-shell NPs, mole ratio of Au:Pd is 1:0.5, incubation at 37 °C for 48 h) is compared with biosynthesized single metal and bimetal nanocatalysts fabricated in the same condition. As is shown in Fig. 6c, single metal (Au or Pd) could also displays higher catalytic activity than blank sample while relatively lower conversion and selectivity is observed when compared with bimetal (Au—Pd) nanocatalysts [56]. Acting as the key factors for operative catalytic process, decomposition of H_2O_2 and generation of highly oxidative ·OH have great influence on consumption of benzyl alcohol [57]. The synergistic effect [58] between Au and Pd NPs have realized efficient charge transfer for these two steps so that production of benzaldehyde would be enhanced [59] while similar selectivity is also detected [60]. Furthermore, it is also found that all the Au, Pd and Au—Pd NPs synthesized by *At*PCS1-*E. coli* have exhibited higher conversion than by wt*E. coli*. Although Au-Pd/wt*E. coli* has also shown catalytic activity to a certain degree [27], poor affinity towards Au^{3+} results in decreased yield of Au—Pd core-shell NPs together with lower conversion. On the contrary, expression of PCs within *At*PCS1-*E. coli* does help to fabrication of more nanocatalysts and improvement of catalytic reaction.

4. Conclusion

In this article, improved biosynthesis of Au-Pd/*At*PCS1-*E. coli* for catalytic enhanced CL and BAO is reported. Through insertion of the gene sequence of *At*PCS1 into the pET-28b vector of *E. coli*, characteristic expression of *At*PCS1 and synthesis of PCs could be realized within *At*PCS1-*E. coli*, which has achieved enrichment of Au^{3+}, higher yield of Au—Pd core-shell NPs accompanied with enhanced CL emission of H_2O_2-luminol system and catalytic activity of H_2O_2-benzyl alcohol system comparing with Au-Pd/wt*E. coli*. During the biosynthetic

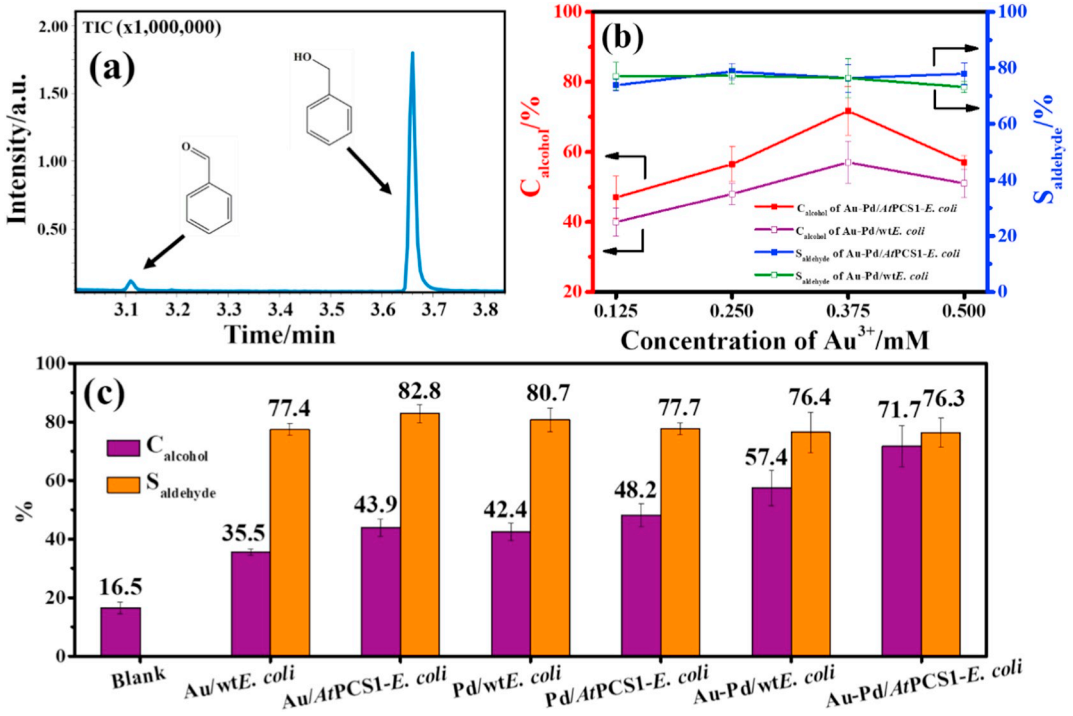

Fig. 6. BAO test of H_2O_2-benzyl alcohol system catalyzed by biosynthesized Au—Pd core-shell NPs under different experiment conditions. (a) GCMS total ions chromatograph of H_2O_2-benzyl alcohol-Au-Pd/*At*PCS1-*E. coli* system; (b) $C_{alcohol}$ and $S_{aldehyde}$ of H_2O_2-benzyl alcohol-catalyst system with different concentration of Au^{3+} from 0.125 to 0.5 mM; (c) $C_{alcohol}$ and $S_{aldehyde}$ of H_2O_2-benzyl alcohol-catalyst system with single metal (Au or Pd) and bimetal (Au—Pd) nanocatalysts biosynthesized with *At*PCS1-*E. coli* or wt*E. coli*.

process, *At*PCS1-*E. coli* on the one hand generates Au—Pd core-shell NPs by itself, on the other hand provides plentiful active sites of PCs for well dispersion of obtained NPs. Besides, the CL effect of H_2O_2-luminol system with Au-Pd/wt*E. coli* under different experimental conditions has displayed stronger CL intensity. In addition, BAO test with Au-Pd/wt*E. coli* under different experimental conditions also exhibited enhanced catalytic activity. It is deduced that the multifunctional PCs contribute to improved biosynthesis of Au—Pd core-shell NPs with better distribution, higher yield and lower cost, which has provided an eminent alternative to traditional chemosynthesis and catalytic application thus further technological improvement and practical application are foreseeable.

Author contributions

The manuscript was written through contributions of all authors. All authors have given approval to the final version of the manuscript.

Declaration of Competing Interest

The authors declare no competing financial interests.

Acknowledgements

We thank Prof. Toshihiro Kogure and Dr. Fumiko Ishizuna in the University of Tokyo for their invaluable help to use electron microscopes.

Appendix A. Supplementary data

Supplementary data to this article can be found online at https://doi.org/10.1016/j.jinorgbio.2019.110795.

References

[1] V. Celorrio, P.M. Quaino, E. Santos, J. Flórez-Montaño, J.J.L. Humphrey, O.G. Villafuerte, D. Plana, M.J. Lázaro, E. Pastor, D.J. Fermin, ACS Catal. 7 (2017) 1673–1680.
[2] C. Fernández-Navarro, S.J. Mejia-Rosales, J. Phys. Chem. C 121 (2017) 21658–21664.
[3] N. Agarwal, S.J. Freakley, R.U. McVicker, S.M. Althahban, N. Dimitratos, Q. He, D.J. Morgan, R.L. Jenkins, D.J. Willock, S.H. Taylor, C.J. Kiely, G.J. Hutchings, Science 358 (2017) 223–227.
[4] P. García-Domínguez, C. Nevado, J. Am. Chem. Soc. 138 (2016) 3266–3269.
[5] S.C. Hsu, Y.C. Chuang, B.T. Sneed, D.A. Cullen, T.W. Chiu, C.H. Kuo, Nano Lett. 16 (2016) 5514–5520.
[6] L. Kesavan, G.J. Hutchings, Science 331 (2011) 195–199.
[7] M.B. Gawande, A. Goswami, T. Asefa, H. Guo, A.V. Biradar, D.L. Peng, R. Zboril, R.S. Varma, Chem. Soc. Rev. 44 (2015) 7540–7590.
[8] P. Zhang, Y. Xiahou, W. Jin, L. Hang, D. Wang, H. Xia, J. Mater. Chem. A 5 (2017) 6992–7000.
[9] X. Jing, W. Tim, L. Ping, H. Chongheng, Y. Jianguo, Y. Weikang, H. Yi-Fan, J. Am. Chem. Soc. 132 (2010) 10398–10406.
[10] S. Cheong, L. Graham, G.L. Brett, A.M. Henning, J. Watt, P.J. Miedziak, M. Song, Y. Takeda, S.H. Taylor, R.D. Tilley, Chemsuschem 6 (2013) 1858–1862.
[11] F. Galvanin, M. Sankar, S. Cattaneo, D. Bethell, V. Dua, G. Hutchings, A. Gavriilidis, Chem. Eng. J. 342 (2018) 196–210.
[12] R. Su, R. Tiruvalam, Q. He, N. Dimitratos, L. Kesavan, C. Hammond, J.A. Lopez-Sanchez, R. Bechstein, C.J. Kiely, G.J. Hutchings, ACS Nano 6 (2012) 6284–6292.
[13] L. Zhang, Z. Xie, J. Gong, Chem. Soc. Rev. 45 (2016) 3916–3934.
[14] P. Mohanpuria, N.K. Rana, S.K. Yadav, J. Nanopart. Res. 10 (2008) 507–517.
[15] T. Park, K.G. Lee, S. Lee, Appl. Microbiol. Biotechnol. 100 (2016) 521–534.
[16] E. Marsili, S.K. Das, Enzym. Microb. Technol. 95 (2016) 1–3.
[17] Z.Y. Wu, H.W. Liang, L.F. Chen, B.C. Hu, S.H. Yu, Acc. Chem. Res. 49 (2015) 96–105.
[18] T. Yamaguchi, Y. Tsuruda, T. Furukawa, L. Negishi, Y. Imura, S. Sakuda, E. Yoshimura, M. Suzuki, Materials 9 (2016) 855–867.
[19] A.D. Chaturvedi, D. Pal, S. Penta, A. Kumar, World J. Microbiol. Biotechnol. 31 (2015) 1595–1603.
[20] K. Fumiya, K. Yugo, F. Kazuo, K. Toshihiro, I. Yuki, Y. Etsuro, S. Michio, Sci. Rep. 6 (2016) 34626–34634.
[21] K.K. Sakimoto, A.B. Wong, P. Yang, Science 351 (2016) 74–77.
[22] C. Luo, V. Shanmugam, C. Yeh, NPG Asia Mater. 7 (2015) 209–220.
[23] J. Liu, Y. Zheng, Z. Hong, K. Cai, F. Zhao, H. Han, Sci. Adv. 2 (2016) 1–8.
[24] H. Chen, D. Sun, X. Jiang, X. Jing, F. Lu, T. Odoomwubah, Y. Zheng, J. Huang, Q. Li, RSC Adv. 3 (2013) 15389–15395.
[25] D.T. Tran, I.P. Jones, J.A. Preece, R.L. Johnston, K. Deplanche, L.E. Macaskie, Nanotechnology 23 (2012) 1–8.

[26] H. Baharak, S.B. Lina Sveidal, R. Amelia-Elena, E. Giti, S. Troels, M. Rikke Louise, Biotechnol. Bioeng. 109 (2011) 45–52.
[27] K. Deplanche, J.A. Bennett, M. Merroun, H. Mounzer, J. Wood, L.E. Macaskie, Top. Catal. 54 (2011) 1110–1114.
[28] A.L. Pochodylo, L. Aristilde, Environ. Chem. Lett. 15 (2017) 1–6.
[29] Z. He, J. Li, H. Zhang, M. Ma, Plant Sci. 168 (2005) 309–318.
[30] N. Chaurasia, Y. Mishra, L. Rai, Biochem. Biophys. Res. Commun. 376 (2008) 225–230.
[31] T.J. Park, S.Y. Lee, N.S. Heo, T.S. Seo, Angew. Chem. Int. Ed. 49 (2010) 7019–7024.
[32] O. Vatamaniuk, S. Mari, Y.P. Lu, P.A. Rea, PNAS 96 (1999) 7110–7115.
[33] S. Wojas, S. Clemens, J. Hennig, A. Skiodowska, E. Kopera, H. Schat, W. Bal, D.M. Antosiewicz, J. Exp. Bot. 59 (2008) 2205–2219.
[34] S. Kumar, M. Abyaneh, S. Gosavi, S. Kulkarni, A. Ahmad, M. Khan, Biotechnol. Appl. Biochem. 47 (2007) 191–195.
[35] E. Grill, S. Löffler, E. Winnacker, M.H. Zenk, PNAS 86 (1989) 6838–6842.
[36] S. Ogawa, T. Yoshidomi, E. Yoshimura, J. Inorg. Biochem. 105 (2011) 111–117.
[37] D. Zhang, T. Yamamoto, D. Tang, Y. Kato, S. Horiuchi, S. Ogawa, E. Yoshimura, M. Suzuki, Talanta 195 (2019) 447–455.
[38] T. Niide, M. Goto, N. Kamiya, Chem. Commun. 47 (2011) 7350–7352.
[39] K. Deplanche, M.L. Merroun, M. Casadesus, D.T. Tran, I.P. Mikheenko, J.A. Bennett, J. Zhu, I.P. Jones, G.A. Attard, J. Wood, J. R. Soc. Interface 9 (2012) 1705–1712.
[40] M. Gholami-Shabani, M. Shams-Ghahfarokhi, Z. Gholami-Shabani, A. Akbarzadeh, G. Riazi, S. Ajdari, A. Amani, M. Razzaghi-Abyaneh, Process Biochem. 50 (2015) 1076–1085.
[41] X. Li, Z. Wang, Z. Zhang, G. Yang, M. Jin, Q. Chen, Y. Yin, Mater. Horiz. 4 (2017) 584–590.
[42] H. Yang, L. Lin, T. Odoom-Wubah, D. Huang, D. Sun, J. Huang, Q. Li, Sep. Purif. Technol. 133 (2014) 380–387.
[43] K. Deplanche, G.A. Attard, L.E. Macaskie, Adv. Mater. Res. 20 (2007) 647–650.
[44] S. Veeraapandian, S.N. Sawant, M. Doble, J. Biomed. Nanotechnol. 8 (2012) 140–148.
[45] S. De Corte, T. Hennebel, J.P. Fitts, T. Sabbe, V. Bliznuk, S. Verschuere, D. van der Lelie, W. Verstraete, N. Boon, Environ. Sci. Technol. 45 (2011) 8506–8513.
[46] L. Du, J. Hong, X. Liu, E. Wang, Electrochem. Commun. 9 (2007) 1165–1170.
[47] T.S.A. Heugebaert, S.D. Corte, T. Sabbe, T. Hennebel, W. Verstraete, N. Boon, C.V. Stevens, Tetrahedron Lett. 53 (2012) 1410–1412.
[48] B. Hosseinkhani, L.S. Søbjerg, A.E. Rotaru, G. Emtiazi, T. Skrydstrup, R.L. Meyer, Biotechnol. Bioeng. 109 (2011) 45–52.
[49] K. Deplanche, L.E. Macaskie, Biotechnol. Bioeng. 99 (2010) 1055–1064.
[50] J. Liu, Q. Yuan, H. Zhao, S. Zou, Catal. Lett. 148 (2018) 1093–1099.
[51] G.D. Yadav, C.K. Mistry, J. Mol. Catal. A Chem. 172 (2001) 135–149.
[52] Z. Wei, D. Liu, W. Wei, X. Chen, Q. Han, W. Yao, X. Ma, Y. Zhu, ACS Appl. Mater. Interfaces 9 (2017) 15533–15540.
[53] V.R. Choudhary, A. Dhar, P. Jana, R. Jha, B.S. Uphade, Green Chem. 7 (2005) 768–770.
[54] S.D. Corte, T. Hennebel, B.D. Gusseme, W. Verstraete, N. Boon, Microb. Biotechnol. 5 (2011) 5–17.
[55] S. Meenakshisundaram, D. Nikolaos, P.J. Miedziak, P.P. Wells, C.J. Kiely, G.J. Hutchings, Chem. Soc. Rev. 41 (2012) 8099–8139.
[56] Y. Chen, H. Lim, Q. Tang, Y. Gao, T. Sun, Q. Yan, Y. Yang, Appl. Catal. A Gen. 380 (2010) 55–65.
[57] I. Moreno, N.F. Dummer, J.K. Edwards, M. Alhumaimess, M. Sankar, R. Sanz, P. Pizarro, D.P. Serrano, G.J. Hutchings, Catal. Sci. Technol. 3 (2013) 2425–2434.
[58] J. Pritchard, L. Kesavan, M. Piccinini, Q. He, R. Tiruvalam, N. Dimitratos, J.A. Lopez-Sanchez, A.F. Carley, J.K. Edwards, C.J. Kiely, Langmuir 26 (2010) 16568–16577.
[59] C.Y. Ma, B.J. Dou, J.J. Li, J. Cheng, Q. Hu, Z.P. Hao, S.Z. Qiao, Appl. Catal. B Environ. 92 (2009) 202–208.
[60] K.R. Seddon, A. Stark, Green Chem. 4 (2002) 119–123.